Journal of Solid State Chemistry **166,** 15–23 (2002)
doi:10.1006/jssc.2002.9545, available online at http://www.idealibrary.com on IDEAL®

The Crystal Structure of $Sr_2TiSi_2O_8$

Thomas Höche,*,[1] Wolfgang Neumann,* Saeid Esmaeilzadeh,† Reinhard Uecker,‡ Markus Lentzen,§ and Christian Rüssel¶

*Lehrstuhl für Kristallographie, Institut für Physik, Humboldt-Universität zu Berlin, Invalidenstraße 110, D-10115 Berlin, Germany; †Arrhenius Laboratory, Department of Inorganic Chemistry, Stockholm University, S-106 91 Stockholm, Sweden; ‡Institut für Kristallzüchtung, Max-Born-Straße 2, D-12489 Berlin, Germany; §Institut für Festkörperforschung, Forschungszentrum Jülich GmbH, D-52425 Jülich, Germany; and ¶Otto-Schott-Institut für Glaschemie, Friedrich-Schiller-Universität, Fraunhoferstrasse 6, D-07743 Jena, Germany

Received October 10, 2001; in revised form February 8, 2002; accepted February 15, 2002

$Sr_2TiSi_2O_8$ single crystals were grown by Czochralski pulling and from a high-temperature solution. X-ray diffractometry revealed the modulated crystal structure of $Sr_2TiSi_2O_8$ to belong to the 5D superspace group *P4bm* ($-\alpha$, α, 1/2; α, α, 1/2) with $\alpha = 0.3$. Atomic positions, anisotropic displacement factors and positional modulation parameters for $Sr_2TiSi_2O_8$ are determined and discussed. The positional modulation is further investigated by electron diffraction and high-resolution transmission electron microscopy. In the latter experiments, the 2D modulation appears to be superimposed by some 1D modulation waves. This effect is discussed in terms of growth conditions. © 2002 Elsevier Science (USA)

Key Words: **$Sr_2TiSi_2O_8$; incommensurate modulation; aperiodic structure; modulation domain boundaries; single-crystal growth; high-resolution transmission electron microscopy; fresnoite.**

1. INTRODUCTION

In fresnoite, $Ba_2TiSi_2O_8$ (1) (space group *P4bm* (2, 3), $a = 0.8529$ nm and $c = 0.5211$ nm (4)), corner-linked TiO_5 pentahedra and pyrosilicate groups, Si_2O_7, comprise flat sheets perpendicular to the [001]-direction (Fig. 1). These sheets are interconnected by 10-fold coordinated barium ions.

$Sr_2TiSi_2O_8$ is assumed to be isotypic with $Ba_2TiSi_2O_8$; however, no structure determination based on single-crystal data has been performed yet. This is because single crystals are much harder to grow compared to $Ba_2TiSi_2O_8$. The substitution of barium by strontium significantly changes the structure of the melts as in quenched $Ba_2TiSi_2O_8$ melts, the majority of Ti^{4+} is five-fold coordinated (20–25% $^{[4]}Ti^{4+}$, 60% $^{[5]}Ti^{4+}$, 15–20% $^{[6]}Ti^{4+}$) (5, 6) whereas in $Sr_2TiSi_2O_8$ glass, six-fold coordinated $^{[6]}Ti^{4+}$ (60%) outweighs $^{[5]}Ti^{4+}$ (40%) and no $^{[4]}Ti^{4+}$ is to be detected (7). This is an indication that the quasibinary phase diagrams Si_2TiO_6–SrO and Si_2TiO_6–BaO significantly differ. The lattice parameters of $Sr_2TiSi_2O_8$ determined by X-ray powder diffraction are: $a = 0.8322$ nm and $c = 0.5029$ nm (JCPDS 39-228).

In contrast to $Ba_2TiSi_2O_8$ (8–10), $Sr_2TiSi_2O_8$ has never been considered for hydrophon and other piezoelectric applications. However, its potential for second harmonic generation has been demonstrated at textured $Sr_2TiSi_2O_8$ films obtained by surface crystallization of a glass (11).

Recently, Höche *et al.* (12) demonstrated that $Sr_2TiSi_2O_8$ hosts incommensurate structural modulations. The latter are also observed in $Ba_2TiSi_2O_8$ (13) and $Ba_2TiGe_2O_8$ (14, 15). Using a Rietveld-refinement of X-ray diffraction data, Iijima *et al.* (14) were able to determine deviations from the average $Ba_2TiGe_2O_8$ structure as they found that the Ge–O–Ge bond angle in the pyrogermanate groups to deviate by $\pm 10^\circ$ from the expected 180°. Markgraf *et al.* (15) proposed a lock-in transition to cause the unusual behavior of permittivity and pyroelectric coefficient in $Ba_2TiGe_2O_8$. In contrast to the structurally very closely related melilites (16–20), the incommensurate structure of neither $Sr_2TiSi_2O_8$, $Ba_2TiGe_2O_8$, nor $Ba_2TiSi_2O_8$ has been solved yet in terms of a superspace representation (21, 22).

In this contribution, we present the results of a single-crystal structure determination performed at $Sr_2TiSi_2O_8$ single crystals grown from a non-stoichiometric melt by the Czochralski pulling technique and using an $SrBr_2$ flux. The modulated structure in $Sr_2TiSi_2O_8$ is assessed in (3 + 2) superspace on the basis of X-ray diffractometer data and compared to electron-diffraction patterns.

2. EXPERIMENTAL

2.1. Sample Preparation

$Sr_2TiSi_2O_8$ crystals have been prepared by three techniques including Czochralski pulling, flux growth, and electrochemically induced nucleation.

[1]To whom correspondence should be addressed. Fax: + + 49-(0)-345-55-27-212. E-mail: thomas.hoeche@physik.hu-berlin.de.

0022-4596/02 $35.00

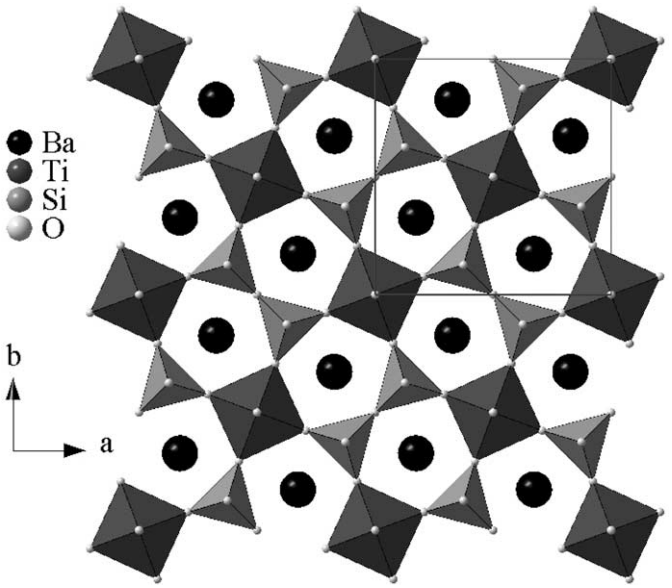

FIG. 1. Crystal structure of fresnoite. Corner-linked SiO_4 tetrahedra and TiO_5 square pyramids make (001) sheets susceptible to rigid unit mode vibrations which freeze in to form incommensurate modulations.

2.1.1. *Czochralski Pulling*

Crystals of $Sr_2TiSi_2O_8$ have been grown using the automated Czochralski pulling technique with rf induction heating. Due to the high melting temperature of this material, an iridium crucible had to be used and therefore the growth was performed under flowing argon. Pulling rates of 0.5 mm h^{-1} and a crystal rotation of 10 min^{-1} were chosen. The axial temperature gradient above the melt was adjusted to about 10 K cm^{-1} by applying an active afterheater. Because of the lack of a seed, an iridium rod was used for seeding.

$Sr_2TiSi_2O_8$ crystals could not be grown from the stoichiometric melt. Therefore, different melt compositions were scrutinized for their crystal-growth suitability. Because the stoichiometric melt led to a mixture consisting of 90% $SrTiO_3$ and only 10% $Sr_2TiSi_2O_8$, the main variation of the melt composition concerned the SiO_2 content. It was increased to about 48 mol%. Nevertheless, no single crystals could be obtained. Only polycrystalline material grew consisting of grains of different phases. The highest $Sr_2TiSi_2O_8$ content (95%) was achieved from melt compositions consisting of 33–35 mol% SrO, 17–19.5 mol% TiO_2 and about 48 mol% SiO_2. The accompanying phases were $SrTiO_3$, rutile, and/or SiO_2. The $Sr_2TiSi_2O_8$ crystals were bluish and clear.

2.1.2. *Single-Crystal Growth from High-Temperature Solutions*

High-temperature solutions do not only help growing crystals well below the melting temperature of the desired compound but also facilitate the synthesis of crystals that melt incongruently. 1.22 g $SrBr_2$ and 1.16 g finely ground $Sr_2TiSi_2O_8$ (partly crystallized glass obtained by melting mixed powders of $SrCO_3$ [Merck], TiO_2 [rutile, Merck, optipur] and SiO_2 [quartz] in an inductively heated furnace) were intimately mixed. Since $SrBr_2$ is highly hygroscopic, work was done under protective Ar atmosphere in a glove box. The mixed powder was placed in a Pt boat and covered with a Pt lid prior to transfer into a quartz ampoule. Upon gentle heating, the quartz tube was evacuated to a final pressure of 10 Pa, sealed and heat treated in an electrically heated chamber furnace (heating to 1250°C at 600 K h^{-1}, 2 h soaking at 1250°C, cooling down to 850°C at 5.7 K h^{-1}, subsequently to 650°C at 20 K h^{-1} and finally within 4 h to room temperature). After washing out $SrBr_2$ using distilled water, very transparent, colorless $Sr_2TiSi_2O_8$ single crystals with well-expressed platelet-like habit (maximum edge length: 500 μm) were identified.

2.1.3. *Textured $Sr_2TiSi_2O_8$ Glass-Ceramics*

As described in detail elsewhere for $Ba_2TiSi_2O_8$ (23–26), an $Sr_2TiSi_2O_8$ melt was prepared from mixed powders of $SrCO_3$ (Merck), TiO_2 (rutile, Merck, optipur) and SiO_2

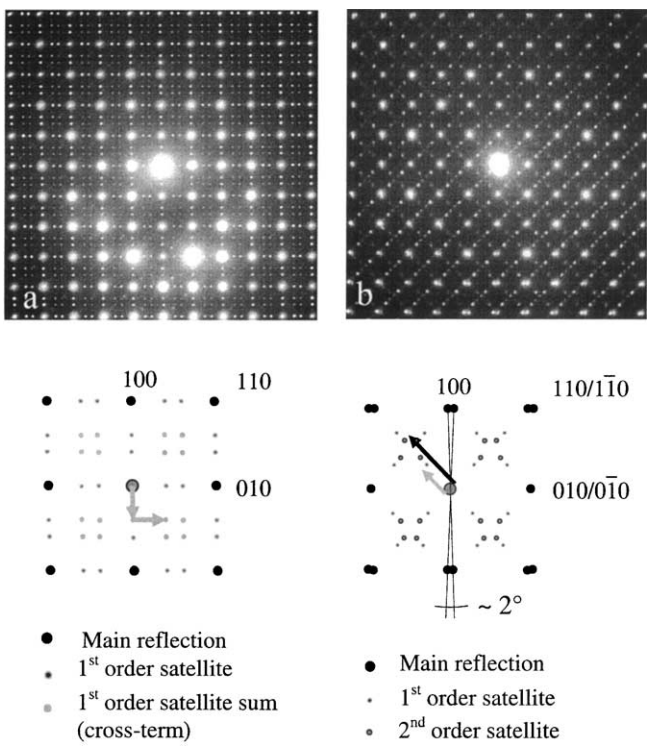

FIG. 2. Selected-area electron diffraction patterns of two different fragments of the Czochralski-pulled $Sr_2TiSi_2O_8$ single crystal together with the corresponding indexing schemes.

(quartz) in an inductively heated furnace. Inside a 250 ml platinum crucible, the melt was homogenized by stirring at 1550°C for 2 h and subsequently soaking for additional 2 h. The Pt crucible was connected to the positive pole of an electric current supply (anode), whereas a platinum plate (which had contact to the negative pole of the current supply) was introduced into the melt in the middle of the crucible (cathode). After carefully supercooling the melt to 1250°C, the current (50 mA) was switched on initiating crystallization at the surface of the cathode. Although the $Sr_2TiSi_2O_8$ crystal-growth rates are much smaller than those observed with $Ba_2TiSi_2O_8$, the same radially textured microstructure found in $Ba_2TiSi_2O_8 \cdot SiO_2$ glass-ceramics (26) occurs.

2.2. Transmission Electron Microscopy

TEM foils were prepared from the glass-ceramics sample by plane-parallel grinding and polishing to about 100 μm thickness, subsequent ultrasonic cutting of 3 mm disks, one-sided dimpling to a residual thickness of about 15 μm and ion beam etching at 2.5 kV acceleration voltage and a beam current (Ar^+ ions) of about 1.2 mA. Static charging of the foil was avoided by the deposition of a very thin carbon layer.

Sub-millimeter-sized single crystals grown by the Czochralski or the flux technique, were crushed and placed on lacey-carbon-film coated copper grids for TEM investigations.

Selected-area electron diffraction (SAED) patterns were recorded using a HITACHI H-8100 II transmission electron microscope operated at 200 kV and high-resolution imaging was carried out with a Philips CM 200 FEG ST microscope operated at an accelerating voltage of 200 kV. The microscope is equipped with a hexapole aberration–correction system, constructed by Haider (27, 28) following a suggestion of Rose (29), which in particular fully compensates the spherical aberration of the objective lens. Images were recorded on a CCD camera at a sampling of 1024×1024 pixels using a spherical aberration of zero and a defocus close to Gaussian focus. In this imaging mode, the optical delocalization is strongly reduced and the residual point spread is mainly determined by the information limit of the instrument, $d = 0.130$ nm.

2.3. X-Ray Diffractometry

A STOE diffractometer with an image-plate detector system (IPDS) and Mo$K\alpha$ radiation was used for the single-crystal X-ray diffraction study. The STOE IPDS software

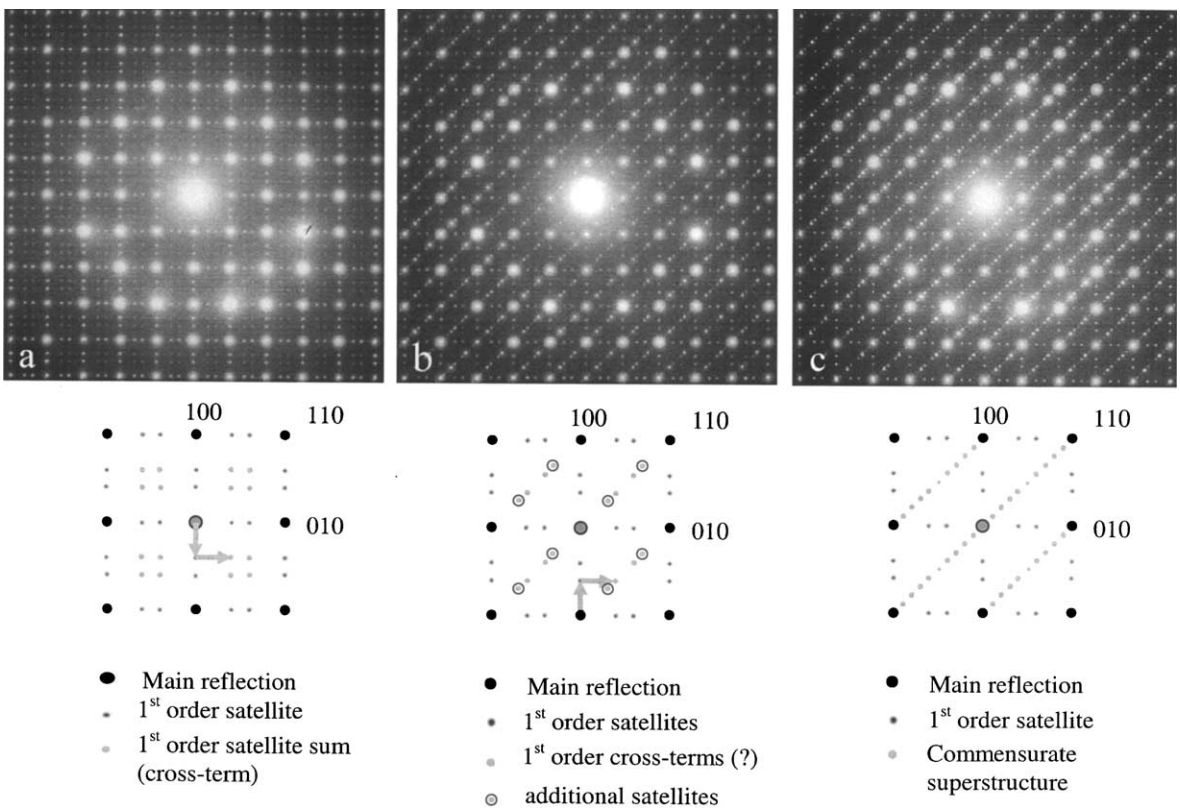

FIG. 3. Selected-area electron diffraction patterns of two different fragments of the flux-grown $Sr_2TiSi_2O_8$ single crystal.

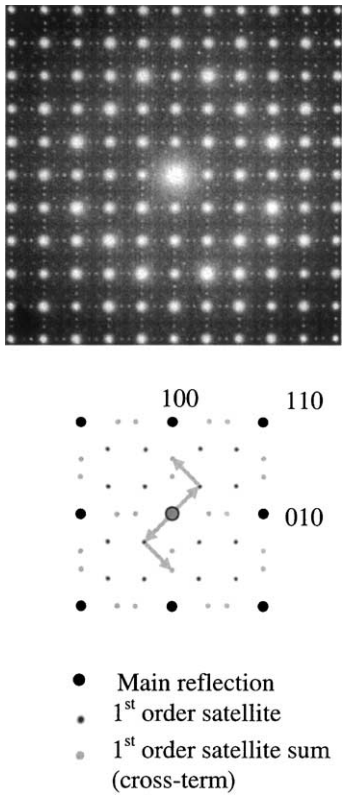

FIG. 4. Selected-area electron diffraction patterns recorded at different positions within the texture-solidified sample prepared by electrochemically induced nucleation.

was employed to integrate reflections belonging to both the average structure as well as the incommensurately modulated superstructure. The software *JANA*98 was used for structure refinement of tetragonal $Sr_2TiSi_2O_8$ with a 2D incommensurate modulation.

3. RESULTS

3.1. Selected-Area Diffraction and TEM Imaging

Similar to the structurally related melilites, structural modulations are very pronounced in (001) planes. Therefore, electron-microscopic investigations were restricted to this projection.

3.1.1. Electron Diffraction

Electron diffraction patterns (EDPs) recorded at different fragments of the *Czochralski* single crystal reveal different positions of the satellite reflections. Both, $\sim 0.4\,0\,0$ (Fig. 2a) and $\sim 0.3 \sim 0.3\,0$ first-order satellites (Fig. 2b) are observed. In Fig. 2b, first-order satellites are accompanied by second-order satellites at $\sim 0.6 \sim 0.6\,0$. Additionally, a splitting of the 100 reflections occur, typical for twinning. The absence of cross-terms in Fig. 2b (the latter are visible in Fig. 2a) indicates that several twin domains, with 1D modulations each but rotated with respect to each other, contribute to this EDP.

At fragments of an $SrBr_2$ *flux-grown* $Sr_2TiSi_2O_8$ single crystal, EDPs similar to that depicted in Fig. 2a clearly dominate (cf. Fig. 3a). In contrast to the sample obtained by Czochralski pulling, no monoclinic distortion was found. In some EDPs, the 2D modulation appears to be superimposed by additional reflections along the [110]-direction (Fig. 3b). In Fig. 3c, this finding is even more clear but in contrast to Fig. 3b, along [110] a 10-fold commensurate superstructure can be recognized.

In the electrochemically nucleated $Sr_2TiSi_2O_8$ *glass-ceramics*, EDPs observed can be classified into two groups: the position of first-order satellites is either located at $\sim 0.4\,0\,0$ (corresponding to Fig. 2a) or at $\sim 0.4 \sim 0.4\,0$ (shown in Fig. 4). In both cases, cross-terms are observed but in contrast to X ray diffraction, double reflection might contribute to electron diffraction patterns. A monoclinic distortion has not been found.

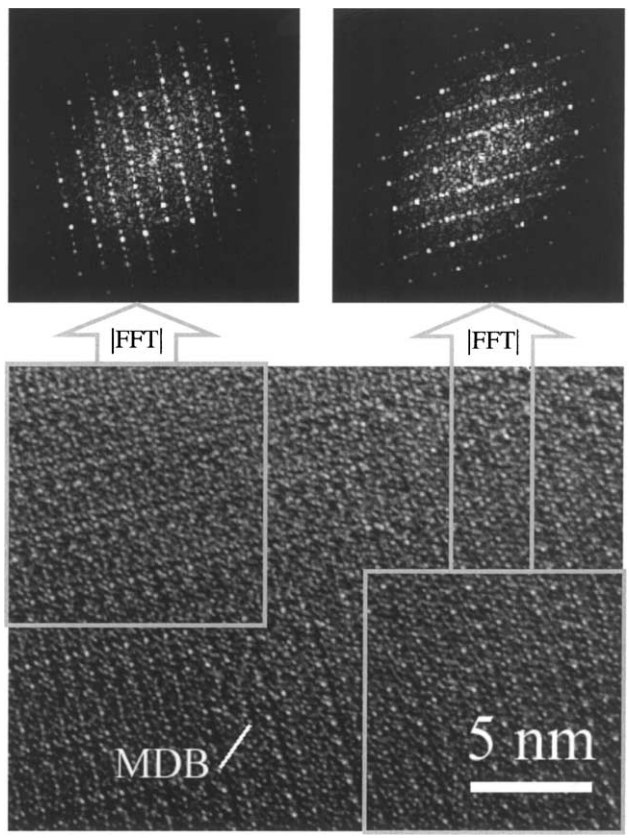

FIG. 5. HRTEM micrograph of a "modulation-domain boundary" (MDB) in $Sr_2TiSi_2O_8$ taken along the [001]-direction. Power spectra proving the 1D modulation are given on top and areas used for their calculation are indicated.

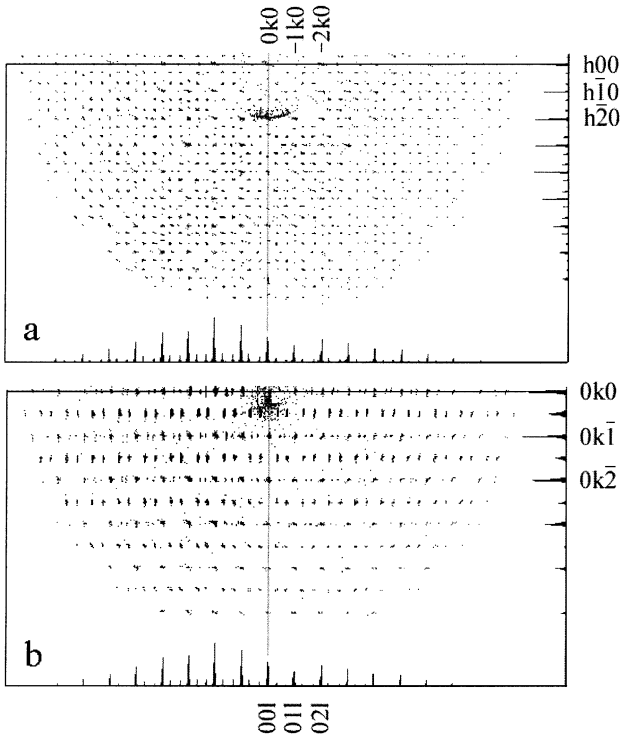

FIG. 6. Projection of the reciprocal space along (a) [001] and (b) [100] (from XRD data).

3.1.2. High-Resolution Imaging

HRTEM inspection of the $Sr_2TiSi_2O_8$ sample prepared by electrochemically induced nucleation highly supports the occurrence of 1D-modulated domains with alternating modulation directions. As indicated by the localized power spectra depicted in Fig. 5, modulation waves possess an inclination close to 90° and the interface between adjacent domains is atomically sharp. The size of the domains ranges between 100 nm and a few micrometers.

3.2. X-Ray Structure Determination

At a small piece of the Czochralski-grown $Sr_2TiSi_2O_8$ sample, the modulated structure of tetragonal $Sr_2TiSi_2O_8$ was refined in the 5D superspace group $P4bm(-\alpha, \alpha, 1/2; \alpha, \alpha, 1/2)\,0gg$ with $\alpha = 0.3$. Although higher-order satellites did exist (in the reciprocal-space projection along [001]* (Fig. 6a), weak cross-terms can be clearly discerned), only harmonic positional modulations of first order were allowed in the analysis. Averaged over all reflections, an *R*-factor of 0.082 was obtained. Further details on data acquisition and structure refinement parameters are compiled in Table 1. Resulting atomic positions and anisotropic displacement parameters for $Sr_2TiSi_2O_8$ are given in Table 2 and the displacive modulation wave parameters are listed in Table 3. In Fig. 7, selected electron-density sections are depicted illustrating that both bridging oxygen ions of the pyrosilicate groups as well as strontium ions experience the strongest positional modulations. The $(3 \times 3 \times 2)$-approximant shown in Fig. 8 illustrates that there is a quite strong distortion of SiO_4 tetrahedra and TiO_5 pyramids are only slightly skewed.

TABLE 1
Data Collection and Crystal Parameters for $Sr_2TiSi_2O_8$

Crystal data	
Chemical formula	$Sr_2TiSi_2O_8$
Formula weight ($g\,mol^{-1}$)	407.3
Superspace group	$P4bm(-\alpha, \alpha, 1/2; \alpha, \alpha, 1/2)0gg$
a (Å)	8.312(2)
c (Å)	10.07(1)
Modulation wave vectors	
q_1	[0.30, 0.30, 0]*
q_2	[-0.30, 0.30, 0]*
V (Å^3)	695.7(2)
ρ ($g\,cm^{-3}$)	3.887
Crystal size	$0.1 \times 0.1 \times 0.1$ mm^3
Crystal color	Transparent white
Data collection	
Diffractometer	STOE IPDS
Radiation type	Mo$K\alpha$
Wavelength (Å)	0.71073
No. of images	200
φ range	0–200°
2θ range	5.5–49°
μ (mm^{-1})	16.8
Data collection method	Phi rotation scans
Absorption correction	Numerical from crystal shape
T_{min}, T_{max}	0.20, 0.29
No. of measured reflections	22,214
No. of independent reflections	1356
No. of observed reflections	748
No. of independent satellites	1053
No. of observed satellites	454
Criterion for observed reflections	$I \geq 3\sigma(I)$
R_{int}	0.096
h, k, l, m, n range	$0 \leq h \leq 6$ $0 \leq k \leq 9$ $-11 \leq l \leq 11$ $-1 \leq m \leq 1$ $-1 \leq n \leq 1$
Refinement	
Refinement on	F
R-factors of all observed reflections R, wR	0.082, 0.080
R-factors of observed main reflections R, wR	0.064, 0.078
R-factors of observed satellites first order: R, wR	0.147, 0.162
Goodness of fit	5.4
No. of reflections used in refinement	748
No. of parameters used in refinement	73
Weighting scheme	$1/(\sigma^2(F) + 0.000025F^2)$
Residual electron density: max., min. (e/Å^3)	6.1, −5.8

TABLE 2
Atomic Positions and Anisotropic Displacement Parameters for $Sr_2TiSi_2O_8$

	x	y	z	U_{11}	U_{22}	U_{33}	U_{12}	U_{13}	U_{23}
Sr	0.32836(4)	0.82836(4)	0	0.0213(3)	0.0213(3)	0.0178(3)	−0.0138(2)	0.0015(3)	0.0015(3)
Ti	0	0	−0.2650(2)	0.0135(6)	0.0135(6)	0.029(1)	0	0	0
Si	0.1293(1)	0.6293(1)	−0.2557(3)	0.0154(7)	0.0154(7)	0.01880(7)	0.0022(7)	−0.003(1)	0.003(1)
O1	0	$\frac{1}{2}$	−0.3129(6)	0.044(5)	0.044(5)	0.029(3)	−0.031(7)	0	0
O2	0.1260(3)	0.6260(3)	−0.0974(4)	0.017(2)	0.017(2)	0.011(2)	0.003(2)	−0.003(1)	−0.003(1)
O3	0.2944(5)	0.5814(7)	−0.3260(4)	0.025(3)	0.136(7)	0.028(2)	0.033(4)	−0.005(2)	0.003(3)
O4	0	0	−0.0984(5)	0.029(3)	0.029(3)	0.009(3)	0	0	0

While the refinement of X-ray diffractometer data acquired at the $SrBr_2$ flux-grown $Sr_2TiSi_2O_8$ single crystal did not reveal significant differences to the results presented above, the quality of the textured glass-ceramics sample did not allow for an X-ray single-crystal structure analysis.

4. DISCUSSION

The analysis of X-ray diffractometer data in terms of a 2D-modulated tetragonal crystal structure resulted in a rather reasonable value of the *R*-factor. Strong absorption, mainly caused by the presence of strontium ions in the crystal, is assumed to be responsible for an *R*-value of the satellite reflections slightly larger than that required. For the same reason, second-order satellites are so weak that they could not be included in the refinement.

Nevertheless, it can be concluded that the structure model depicted in Fig. 8 reflects typical details of the crystal structure. However, electron diffraction and HRTEM experiments performed at $Sr_2TiSi_2O_8$ crystals grown under different conditions indicate that there are parts of the sample possessing a twinned 1D modulation instead of the 2D-modulated structure. Such mixed-dimensional modulations have been reported earlier by van Heurck *et al.* in $Ca_2ZnGe_2O_7$ (30). Since only tiny volumes are investigated by TEM, it is impossible to draw conclusions concerning the ratio of one- and two-dimensionally modulated domains.

The anisotropic displacement parameters for the $Sr_2TiSi_2O_8$ structure (Table 2) are worth considering more closely. The most obvious finding is that U_{22} of O3 is exceptionally large while positional modulation wave parameters for O1 (sine terms in x and y directions) are the largest. In order to discuss these observations, in Fig. 9, anisotropic displacement ellipsoids for the basic structure (refined without considering the modulation) and the modulated average structure are shown. The juxtaposition reveals that the introduction of the modulation leads to a general decrease of the size of the displacement ellipsoids, and in particular, the displacement ellipsoid of position O1 is no longer elongated. The latter finding must be interpreted such that in the non-modulated structure

TABLE 3
Positional Modulation Wave Parameters for $Sr_2TiSi_2O_8$

	Order of modulation	sin			cos		
		x	y	z	x	y	z
Sr	100	−0.0053(2)	0.0053(2)	0	−0.0034(2)	0.0034(2)	0
Sr	010	0.0040(2)	0.0040(2)	0.0048(2)	0.0059(2)	−0.0059(2)	0
Ti	100	0.0121(6)	0.0078(6)	0	0	0	−0.0010(5)
Ti	010	−0.0078(6)	0.0121(6)	0	0	0	−0.0010(5)
Si	100	−0.0035(6)	0.0035(6)	0	−0.0020(6)	−0.0020(6)	0
Si	010	0.0096(6)	0.0096(6)	0.0009(7)	−0.0064(6)	0.0064(6)	0
O1	100	−0.037(2)	0.037(2)	0	0	0	0
O1	010	0.009(2)	0.009(2)	0	0	0	0
O2	100	0.000(1)	0.000(1)	0	−0.003(1)	0.003(1)	0
O2	010	0.006(1)	0.006(1)	0.002(1)	−0.006(1)	0.006(1)	0
O3	100	−0.009(2)	−0.015(2)	0.002(2)	0.012(2)	0.022(2)	0.006(2)
O3	010	0.013(2)	0.008(2)	0.000(2)	0.006(2)	0.025(2)	0.001(2)
O4	100	0.011(2)	0.006(2)	0	0	0	−0.006(1)
O4	010	−0.006(2)	0.11(2)	0	0	0	−0.006(1)

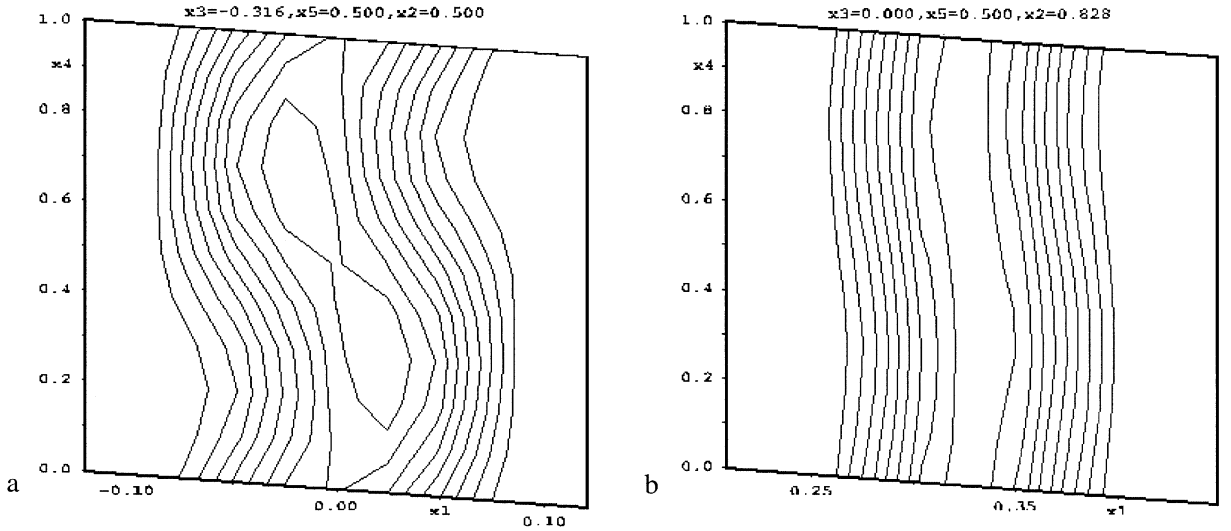

FIG. 7. Electron-density maps modulation dimension x_4 versus real-space dimensions x_1: (a) bridging oxygen ions, and (b) Sr^{2+} ions.

(Fig. 9a), displacements of O1 caused by the positional modulation wave are erroneously described in terms of a statistical uncertainty of the position. The introduction of the modulation wave, however, does describe the behavior of the O1 position more precisely and therefore, the anisotropic displacement ellipsoid appear significantly reduced in Fig. 9b. Nevertheless, position O3 still does possess a highly elongated displacement ellipsoid and inspection of Fig. 9b reveals that the shape of this ellipsoids is likely to result from collective rotations of TiO_5 pyramids and SiO_4 tetrahedra about the crystallographic *c*-axis. A thorough analysis of rigid-unit modes in the fresnoite framework-structure type (31) has shown exactly this coupled rotation/displacement to generate modulation vectors of the type $\mathbf{q} = \varepsilon\langle 110\rangle^*$ with $\varepsilon = 0.315$ (for $Ba_2TiGe_2O_8$) and $\varepsilon = 0.298$ (for $Ba_2TiSi_2O_8$). For $Sr_2TiSi_2O_8$, such modulation wave vectors with $\varepsilon = 0.3$ have been shown in Figs. 2b, 4, and 6 but not in Figs. 2a, 3a–c. The existence of more than one intergrown room-temperature $Sr_2TiSi_2O_8$ polymorph might be caused by the occurrence of particular modulation waves depending on composition, growth conditions, etc.

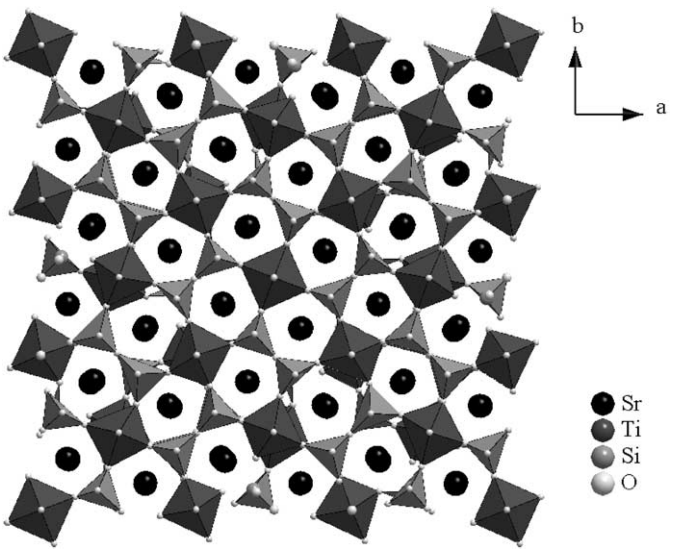

FIG. 8. $3 \times 3 \times 2$ approximant of the modulated crystal structure of $Sr_2TiSi_2O_8$.

For the structurally closely related $(Ca_{1.89}Sr_{0.01}Na_{0.08}K_{0.02})(Mg_{0.92}Al_{0.08})(Si_{1.98}Al_{0.02})O_7$ melilite, Bindi *et al.* described that the positional modulation leading to changes in the coordination (six-fold to eight-fold) around the large cation position (corresponding to strontium in $Sr_2TiSi_2O_8$) gives rise to an additional modulation of the thermal parameters (32). Therefore, in the present $Sr_2TiSi_2O_8$ refinement, thermal parameter modulations were allowed for Sr and O3 site resulting in unchanged *R*-factors for main reflections and an 8% decrease of the satellite-reflection *R*-factor.

Since the introduction of a modulation does only slightly decrease the total lattice energy, modulated structures are very likely to be susceptible to changes imposed by local stresses. Therefore, it cannot be excluded that the 1D modulations observed in the TEM are (in part) artifacts caused by a changed surface-to-volume ratio of the electron-transparent fragments and localized stresses introduced during the preparation process.

In addition to different TEM preparation techniques applied to glass-ceramics and single crystals, very different crystal growth conditions complicate a direct comparison of the demonstrated variation range of structural modulations. It is most likely that growth conditions including growth

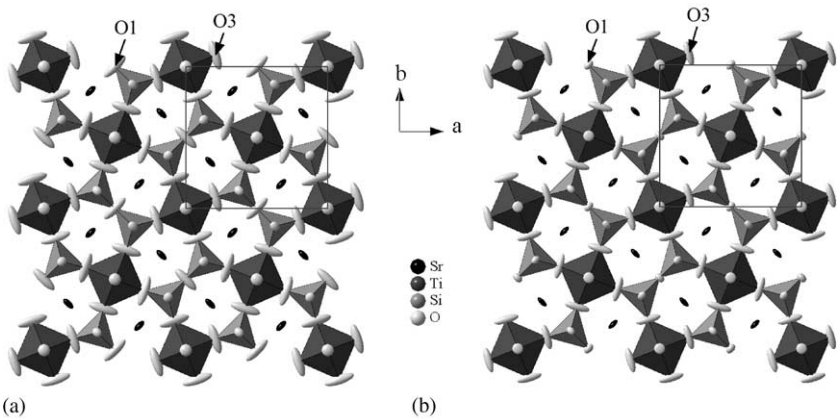

FIG. 9. Average structure of $Sr_2TiSi_2O_8$ with vibrational ellipsoids (on a probability level of 70%): (a) non-modulated structure, and (b) modulated structure with masked out modulation wave.

rate, stoichiometry of the melt, and crystallite size will have a significant influence on the very sensitive modulated structure. Positionally modulated structures are particularly sensitive to changes in composition (33). Therefore, the monoclinic distortion occasionally observed with the Czochralski pulled sample might be correlated to the composition of the non-stoichoimetric melt the crystal was grown from.

The scarcely found modulation-satellite reflections along [110] in the *flux-grown* single crystal (Figs. 3b and c) resemble those observed in $Ba_2TiGe_2O_8$ (14, 15). Recalling the ionic radii of four-fold coordinated silicon (40 pm), germanium (53 pm), and titanium (56 pm), those 1D modulations might be caused by a local substitution of silicon by titanium.

In the glass-ceramics sample, growth rates are several orders of magnitude higher than applied to grow crystals from the flux or by Czochralski pulling. Given the fact that only 40% of the Ti^{4+} is five-fold coordinated in the melt and for the growth of fresnoite, the coordination of the remaining 60% six-fold coordinated $^{[6]}Ti^{4+}$ must be reduced (7). Since this change of coordination required for growth seems to be the factor limiting, the $Sr_2TiSi_2O_8$ growth front to proceed faster through the melt, it is most unlikely that after a further reduction of the coordination of $^{[5]}Ti^{4+}$, $^{[4]}Ti^{4+}$ will substitute for $^{[4]}Si^{4+}$.

The calculation of bond valence sums, BVSs, for all cations in $Sr_2TiSi_2O_8$ according to Brese and O'Keefe (34), clearly show that the Sr^{2+} ions possessing a BVS of 1.525 are drastically underbonded. The introduction of the

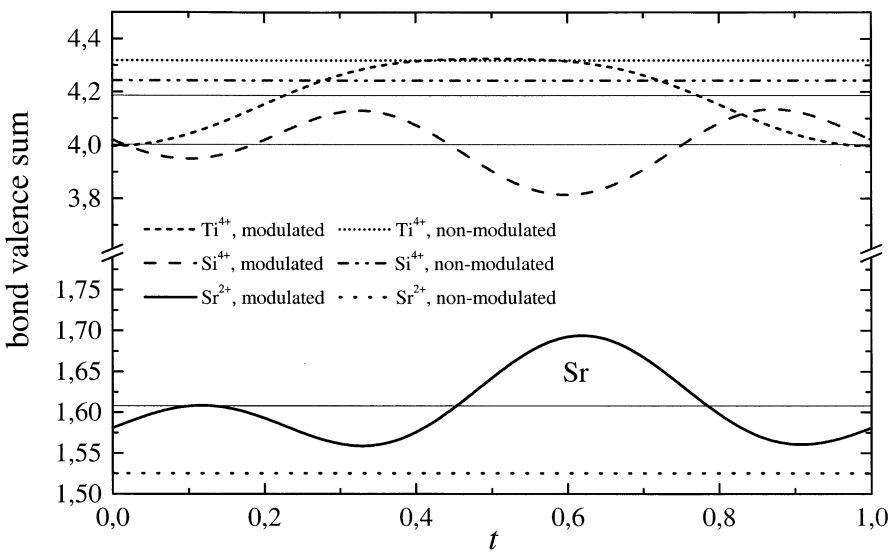

FIG. 10. Bond-valence sums for Sr^{2+}, Ti^{4+} and Si^{2+} in $Sr_2TiSi_2O_8$ for the unmodulated and the modulated structure dependent on the modulation phase *t*.

modulation does significantly improve this unsatisfactory bonding since on the average the Sr^{2+}-BVS then amounts to 1.61 with a maximum of 1.7 (cf. Fig. 10). In parallel, Ti^{4+} as well as Si^{4+} ions can improve their BVSs towards very close to the optimum value. This empirical considerations are in broad agreement with the hypothesis established for melilites (see e.g. (17, 35)) that the modulation is caused by the large cations endeavoring more satisfactory bonding conditions.

5. CONCLUSIONS

$Sr_2TiSi_2O_8$ crystals were grown for the fist time by three techniques including Czochralski pulling, $SrBr_2$ flux growth, and electrochemically induced nucleation. The best single crystal was obtained by the flux technique using a stoichiometric melt blended with $SrBr_2$. X-ray diffractometry identified the five-dimensional supergroup $P4bm$ $(-\alpha, \alpha, 1/2; \alpha, \alpha, 1/2)$ $0gg$ with $\alpha = 0.3$ for $Sr_2TiSi_2O_8$. Neglecting the modulation, $Sr_2TiSi_2O_8$ is isotypic with $Ba_2TiSi_2O_8$ which is much easier to grow since in contrast to $Sr_2TiSi_2O_8$, $Ba_2TiSi_2O_8$ does not melt incongruently. Different crystal-growth techniques lead to subtle changes in the modulated structure. The large underbonding of strontium ions is most likely to be the driving force provoking the positional modulation in $Sr_2TiSi_2O_8$.

ACKNOWLEDGMENTS

The authors Petříček thank Sven Lidin and Václav for discussions on the structure refinement. T.H., W.N., and C.R. acknowledge the financial support by Deutsche Forschungsgemeinschaft Bonn Bad Godesberg (contracts NE 646/8-1, RU 417/6-1). Visits in Jülich were funded within the program "Grossgeräteinitiative Analytische HRTEM" by Deutsche Forschungsgemeinschaft Bonn (NE646/4-1). The project on aberration correction of a transmission electron microscope was funded by Volkswagen Stiftung. S.E. thanks the Blanceflor foundation for financial support. We are indebted to Ralf Keding for contributing the sample synthesized by electrochemically induced nucleation and for valuable discussions.

REFERENCES

1. J. T. Alfors, M. C. Stinton, R. A. Matthews, and A. Pabst, *Amer. Mineral.* **50,** 314–340 (1965).
2. P. B. Moore and S. J. Louisnathan, *Science* **156,** 1361–1362 (1967).
3. R. Masse, J.-C. Grenier, and A. Durif, *Bull. Soc. Franc. Mineral. Cristallogr.* **90,** 20–23 (1967).
4. S. A. Markgraf, A. Halliyal, A. S. Bhalla, and R. E. Newnham, *Ferroelectrics* **62,** 17–26 (1985).
5. F. Farges, *J. Non-Cryst. Solids* **204,** 53–64 (1996).
6. M. Schneider, W. Richter, R. Keding, and C. Rüssel, *J. Non-Cryst. Solids* **226,** 273–280 (1998).
7. M. Schneider, Ph.D. Thesis, Physikalisch-Astronomische Fakultät, Friedrich-Schiller-Universität, Jena, 1998.
8. R. Y. Ting, A. Halliyal, and A. S. Bhalla, *Appl. Phys. Lett.* **44,** 852–854 (1984).
9. A. Halliyal, A. Safari, A. S. Bhalla, and R. E. Newnham, *Ferroelectrics* **50,** 45–50 (1983).
10. A. Halliyal, A. Safari, A. S. Bhalla, R. E. Newnham, and L. E. Cross, *J. Am. Ceram. Soc.* **67,** 331–335 (1984).
11. Y. Ding, N. Masuda, Y. Miura, and A. Osaka, *J. Non-Cryst. Solids* **203,** 88–95 (1996).
12. T. Höche, C. Rüssel, and W. Neumann, *Solid State Commun.* **110,** 651–656 (1999).
13. S. A. Markgraf, C. A. Randall, A. Bhalla, and R. J. Reeder, *Solid State Commun.* **75,** 821–824 (1990).
14. K. Iijima, F. Marumo, M. Kimura, and T. Kawamura, *J. Chem. Soc. Jpn.* **10,** 1557–1563 (1981).
15. S. A. Markgraf and A. Bhalla, *Phase Transitions* **18,** 55–76 (1989).
16. B. S. Hemingway, J. H. T. Evans, J. G. L. Nord, J. H. T. Haselton, R. A. Robie, and J. J. McGee, *Can. Mineral.* **24,** 425–434 (1986).
17. F. Seifert, M. Czank, B. Simons, and W. Schmahl, *Phys. Chem. Miner.* **14,** 26–35 (1987).
18. M. Riester and H. Böhm, *Z. Kristallogr.* **212,** 506–509 (1997).
19. H. Yang, R. M. Hazen, R. T. Downs, and L. W. Finger, *Phys. Chem. Miner.* **24,** 510–519 (1997).
20. J. C. Jiang, M. Schosnig, A. K. Schaper, K. Ganster, H. Rager, and L. Tóth, *Phys. Chem. Miner.* **26,** 128–134 (1998).
21. P. M. de Wolff, T. Janssen, and A. Janner, *Acta Crystallogr. A* **37,** 625–636 (1981).
22. T. Janssen, A. Janner, A. Looijenga-Vos, and P. M. de Wolff, *in* "International Tables for Crystallography" (A. J. C. Wilson, Ed.), Mathematical, Physical and Chemical Tables, Vol. C, pp. 797–844. Kluwer Academic Publishers, Dordrecht, 1995.
23. R. Keding and C. Rüssel, *Ber. Bunsengesell. Phys. Chem.* **100,** 1515–1518 (1996).
24. R. Keding and C. Rüssel, *J. Non-Cryst. Solids* **219,** 136–141 (1997).
25. R. Keding, G. von der Gönna, K. Gerth, and C. Rüssel, *in* "XVIII International Congress on Glass" (M. K. Choudhury, N. T. Huff, and C. H. Drummond III, Eds), Vol. CD-ROM C2, pp. 90–95. The American Ceramic Society, San Francisco, CA, 1998.
26. T. Höche, R. Keding, C. Rüssel, and R. Hergt, *J. Mater. Sci.* **34,** 195–208 (1999).
27. M. Haider, G. Braunshausen, and E. Schwan, *Optik* **99,** 167–179 (1995).
28. M. Haider, H. Rose, S. Uhlemann, E. Schwan, B. Kabius, and K. Urban, *Ultramicroscopy* **75,** 53–60 (1998).
29. H. Rose, *Optik* **85,** 19–24 (1990).
30. C. V. Heurck, G. v. Tendeloo, and S. Amelinckx, *Phys. Chem. Miner.* **18,** 441–452 (1992).
31. R. L. Withers, Y. Tabira, Y. Liu, and T. Höche, *Phys. Chem. Miner.* (2001), submitted for publication.
32. L. Bindi, P. Bonazzi, M. Dusek, V. Petricek, and G. Chapuis, *Acta Crystallogr. Sect. B—Struct. Sci.* **57,** 739–746 (2001).
33. M. Schosnig, A. K. Schaper, A. Kutoglu, W. Treutmann, and H. Rager, *Z. Kristallogr.* **215,** 495–498 (2000).
34. N. E. Brese and M. O'Keeffe, *Acta Crystallogr. B* **47,** 192–197 (1991).
35. J. D. C. McConnell, *Z. Kristallogr.* **214,** 457–464 (1999).